Supporting information for

Dual-Strategy of Carbon-Coating and Nanoengineering Enables Reversible and Durable Na Storage in an Iron-Based Pyrophosphate Cathode

Zhitao Cao[a], Xiaoping Hu[a], Yuyao Wang[a], Yongqing Xu[a], Yifan Zhou[a], Xinxin Cao[a,b,*], and Shuquan Liang[a,b,*]

[a] School of Materials Science and Engineering, Central South University, Changsha 410083, Hunan, China

[b] Key Laboratory of Electronic Packaging and Advanced Functional Materials of Hunan Province, Central South University, Changsha 410083, Hunan, China

*Corresponding Author: caoxinxin@csu.edu.cn (X. Cao); lsq@csu.edu.cn (S. Liang).

Experimental section

Materials preparation

The $Na_{3.12}Fe_{2.44}(P_2O_7)_2$/C (NFPO/C) nanoflakes were synthesized via a solid-state reaction in molten surfactant-paraffin media.[1, 2] Initially, $NH_4H_2PO_4$ (AR, SINOPHARM) was subjected to high-energy ball milling with oleic acid (AR, SINOPHARM) for 0.5 h. Subsequently, paraffin (Aladdin) was added and the mixture was further milled for an additional hour. Then, $FeC_2O_4 \cdot 2H_2O$ (AR, Aladdin) was introduced and the ball milling process continued for 0.5 h. Finally, CH_3COONa (AR, SINOPHARM) was added and the mixture underwent another 2 hours of ball milling to yield a viscous precursor mixture with a molar ratio of Na: Fe: P: oleic acid being 3.12: 2.44: 4: 4. Additionally, the weight of paraffin was twice that of oleic acid. The precursor was calcined at 300 ℃ for 10 hours in an argon (Ar) atmosphere with a heating rate of 2 °C per minute, followed by further elevation to 600 °C for 12 hours to obtain NFPO/C nanoflakes. NFPO-O and NFPO-P cathode materials were prepared using solely oleic acid and paraffin, respectively. Oleic acid served as both a surfactant and carbon source, while paraffin functioned as a hydrophobic nonpolar solvent providing a stable environment for the moisture-sensitive precursors.

Materials characterization

The crystal structure and phase composition of the materials were determined using X-ray diffractometry (XRD, Rigaku Mini Flex 600 with Cu-Kα radiation, λ = 1.5418 Å), and the obtained XRD patterns were refined utilizing the Rietveld method. The morphology, microstructure, and elemental distribution of the samples were characterized employing scanning electron microscopy (SEM, Quanta FEG 250), transmission electron microscopy (TEM, FEI Titan G2 60-300), and high-resolution transmission electron microscopy (HRTEM) coupled with energy dispersive spectrometry (EDS). The composition and valence states of the elements in the samples were characterized using X-ray photoelectron spectroscopy (XPS). The properties and vibrational states of functional groups in the materials were investigated through Raman spectra (LabRAM HR800) and Fourier transform infrared Spectrometer (FT-IR, Nicolet6700). The carbon content of the material was determined by thermogravimetric analysis (TG, Netzsch STA449C) in an air environment. The Brunauer-Emmett-Teller (BET)

surface area and pore size distributions of the materials were obtained from N_2 adsorption/desorption isotherms. In-situ XRD analysis was performed using a customized battery case with an Al foil (5μm) serving as a collector for the cathode electrode. Each scan lasted for 5 minutes while cycling the cell at a rate of 0.4C during charging and discharging processes. Ex-situ XRD analysis was conducted by charging and discharging the battery to different voltages, followed by disassembling it to conduct XRD measurements. Al foil (15μm) was used as the collector for ex-situ XRD analysis.

Electrode preparation and electrochemical measurement

The cathode electrode was prepared by thoroughly grinding a mixture of the active material, Ketjen Black, and polyvinylidene fluoride (PVDF) in a ratio of 7:2:1. An appropriate amount of N-methyl-2-pyrrolidone (NMP) solvent was added to prepare an electrode slurry, which was then applied onto an Al foil (15μm). The coated foil was placed in a vacuum oven at 80°C for overnight drying before being cut into circular electrodes with a diameter of 12 mm. The mass loading of the cathode electrode active material ranged from approximately 1.2 to 1.5 mg cm^{-1}. Sodium metal served as the reference electrode for the half-cell configuration, while a glass fiber membrane acted as the separator between electrodes. The electrolyte was a solution of 1 M $NaClO_4$ in ethylene carbonate (EC)-diethyl carbonate (DEC) (1:1, V/V) with addition of 5 vol% fluorinated ethylene carbonate (FEC). The testing was conducted using CR2025 coin cells, with the cell assembly process performed in a glove box filled with an argon atmosphere. The concentrations of O_2 and H_2O were maintained below 0.1 ppm throughout the process. Galvanostatic charge/discharge measurements were carried out on a multi-channel battery testing system (LAND CT2001A, China) within the potential range of 1.5-4.0 V (relative to Na^+/Na). The cyclic voltammetry (CV) tests in the range of 1.5-4 V (relative to Na^+/Na) and the electrochemical impedance spectroscopy (EIS) tests in the frequency range of 1.0×10^5-1.0×10^{-2} Hz were performed on an electrochemical workstation (Chenhua CHI660E, China).

For the preparation of anode electrode, a mixture of hard carbon (HC), Super P, and PVDF in a ratio of 7:2:1 was thoroughly milled and homogenized with an appropriate amount of NMP solvent. The resulting mixture was then coated onto Cu foil (15μm) and dried overnight in a vacuum oven at 80°C. The CR 2025-type coin cells were subsequently assembled in a glove box filled with high-purity argon, ensuring O_2 and H_2O levels below 0.1 ppm. Prior to full cell

assembly, the hard carbon anode underwent pre-sodiation through 3 pre-cycles at a current density of 1C to establish a stable SEI film and minimize irreversible capacity loss. The HC purchased through Taobao is a product of Kuraray. It is prepared by asphalt, polymers, and plants as raw materials, with a carbonization temperature ranging from 1000 to 1500 ℃. The layer spacing (d(002)) measures between 0.38 and 0.40 nm, while the microcrystal size ranges from 1.1 to 1.2 μm. The N/P ratio between the anode and cathode was approximately 1.1:1. The specific capacity of the full cell was calculated based on the mass of the cathode active material.

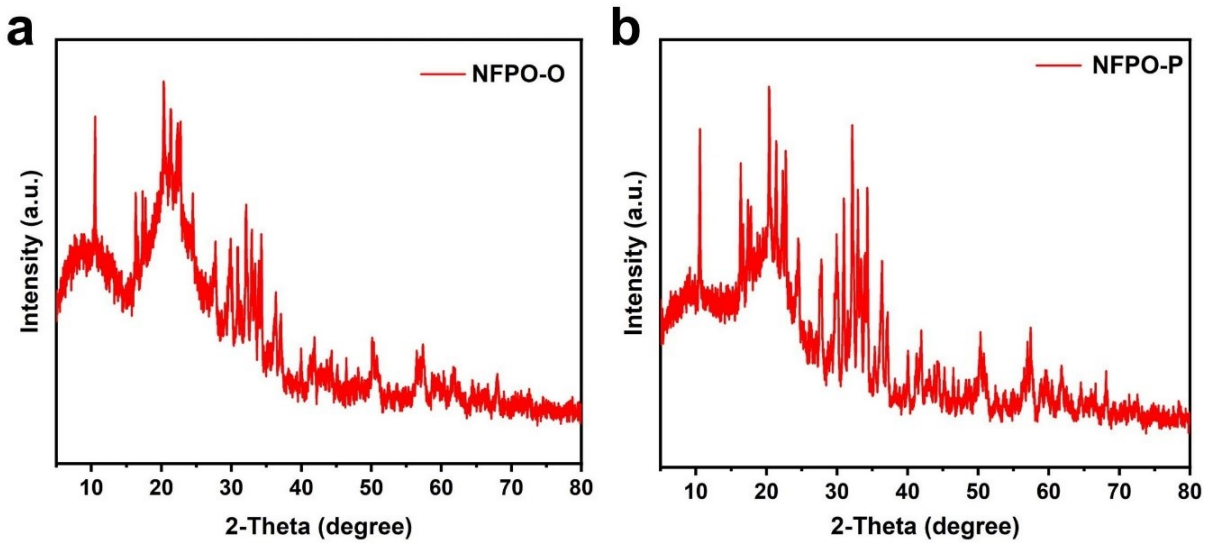

Fig. S1 The powder XRD patterns of (a) NFPO-O, and (b) NFPO-P materials.

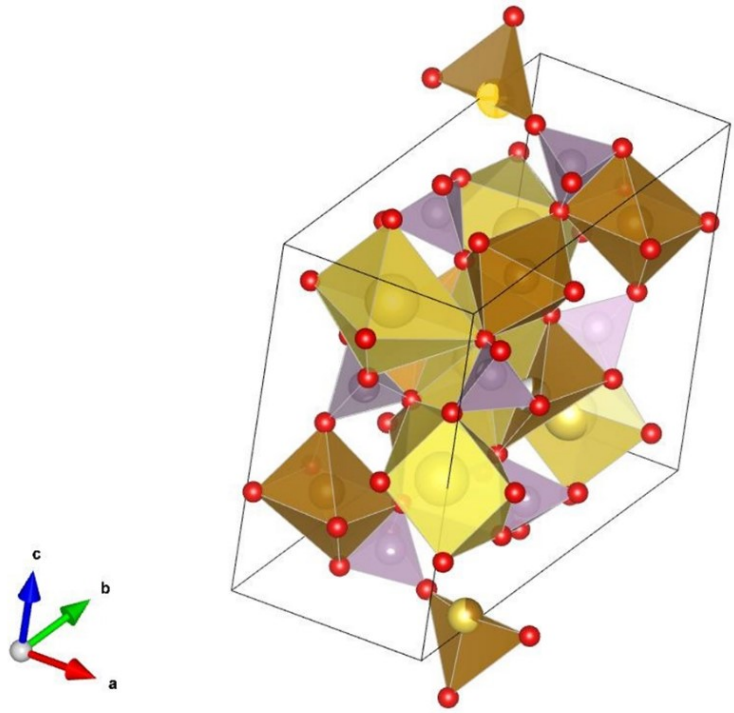

Fig. S2 Schematic illustration of the crystal structure of $Na_{3.12}Fe_{2.44}(P_2O_7)_2$.

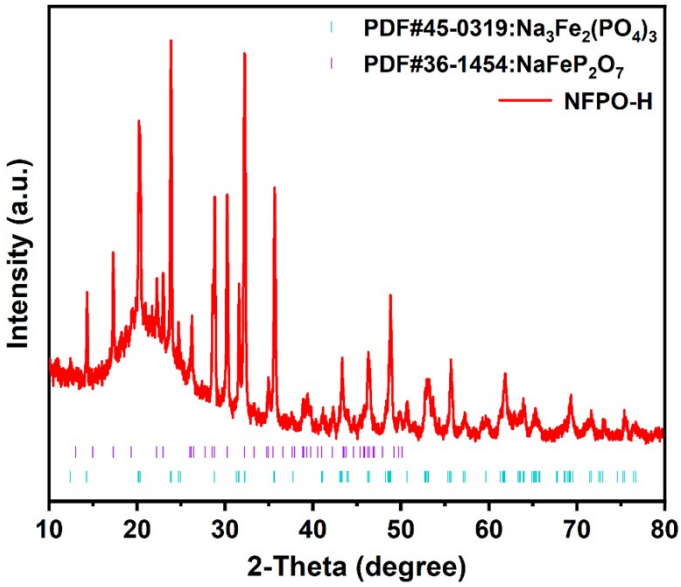

Fig. S3 The XRD pattern of NFPO/C powder after thermogravimetric analysis in air (800 °C).

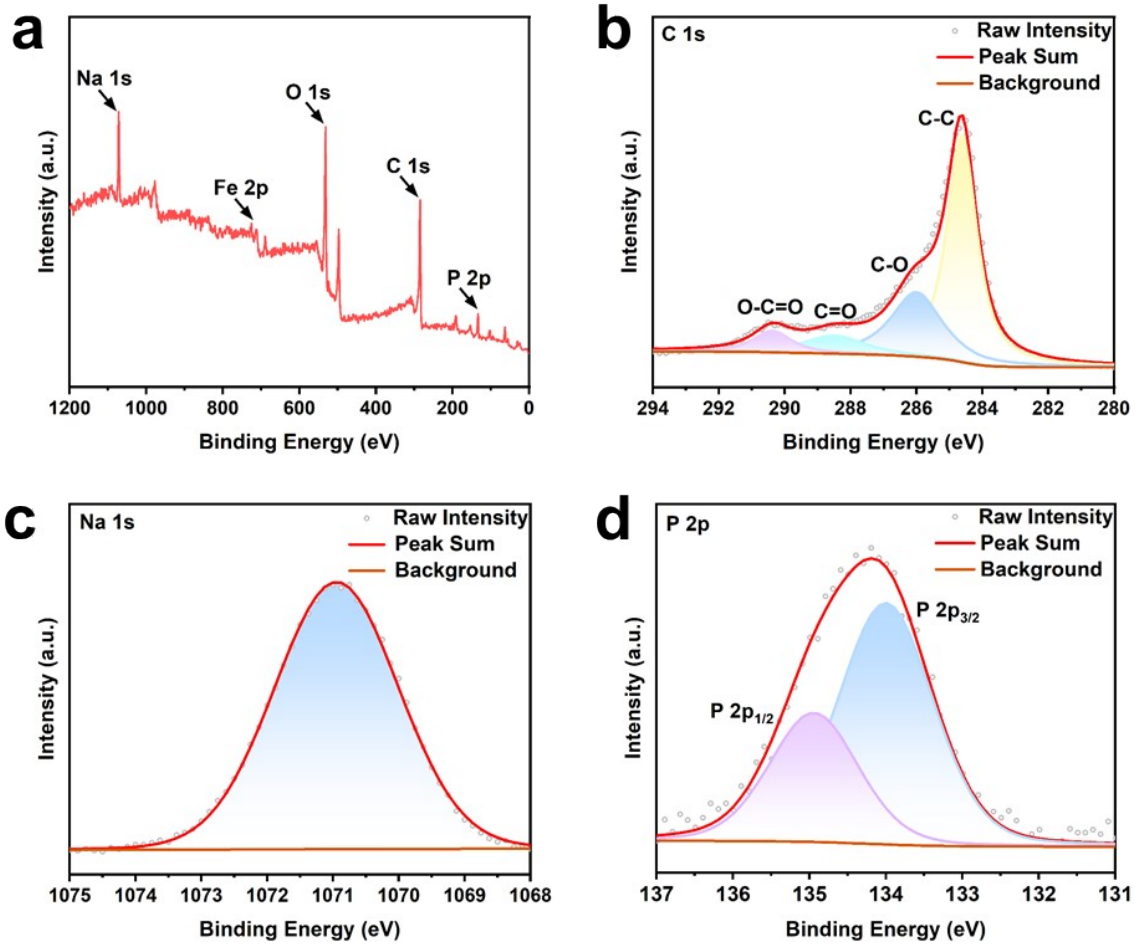

Fig. S4 (a) Typical XPS survey spectrum and the corresponding high-resolution XPS spectra of (b) C 1s, (c) Na 1s, and (d) P 2p in NFPO/C material.

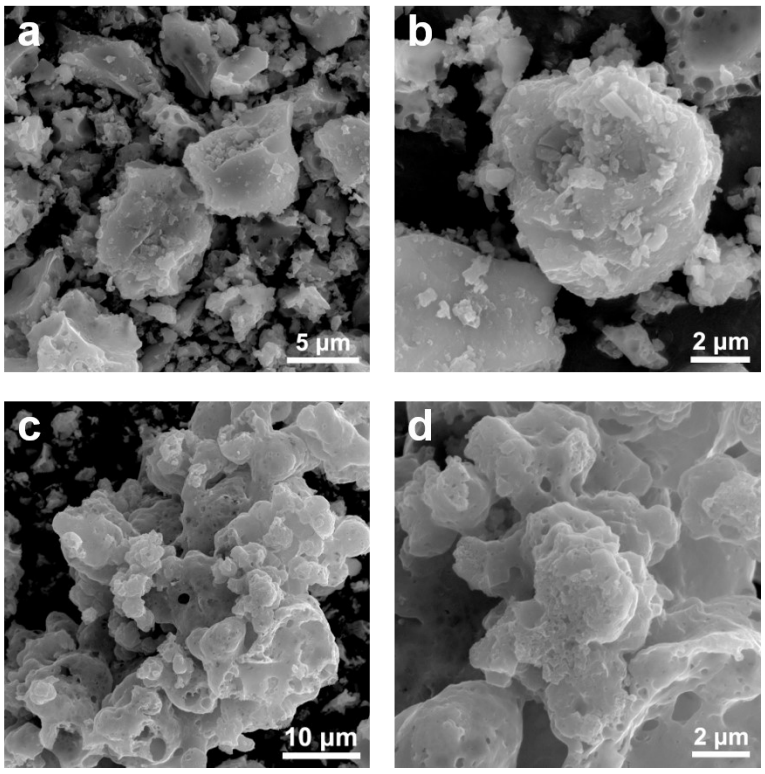

Fig. S5 The SEM images of (a, b) NFPO-O, and (c, d) NFPO-P materials.

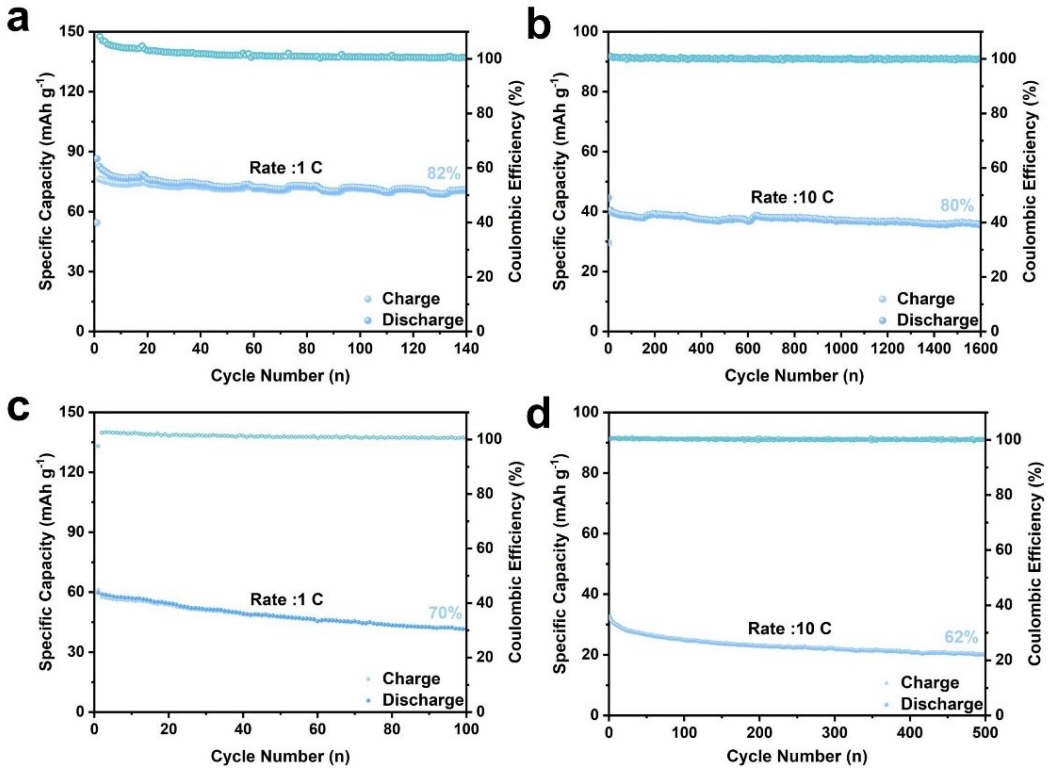

Fig. S6 Cycling performance at 1C and 10 C for the (a, b) NFPO-O electrode, and the (c, d) NFPO-P electrode.

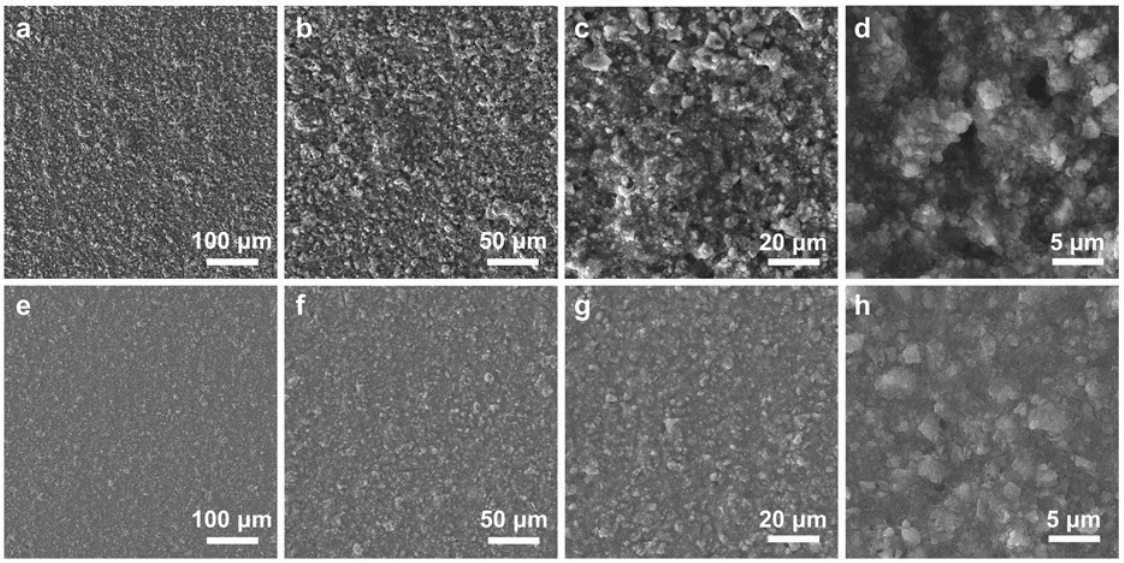

Fig. S7 The SEM images of NFPO/C electrode (a-d) before cycling, and (e-h) after 200 cycles at 5 C.

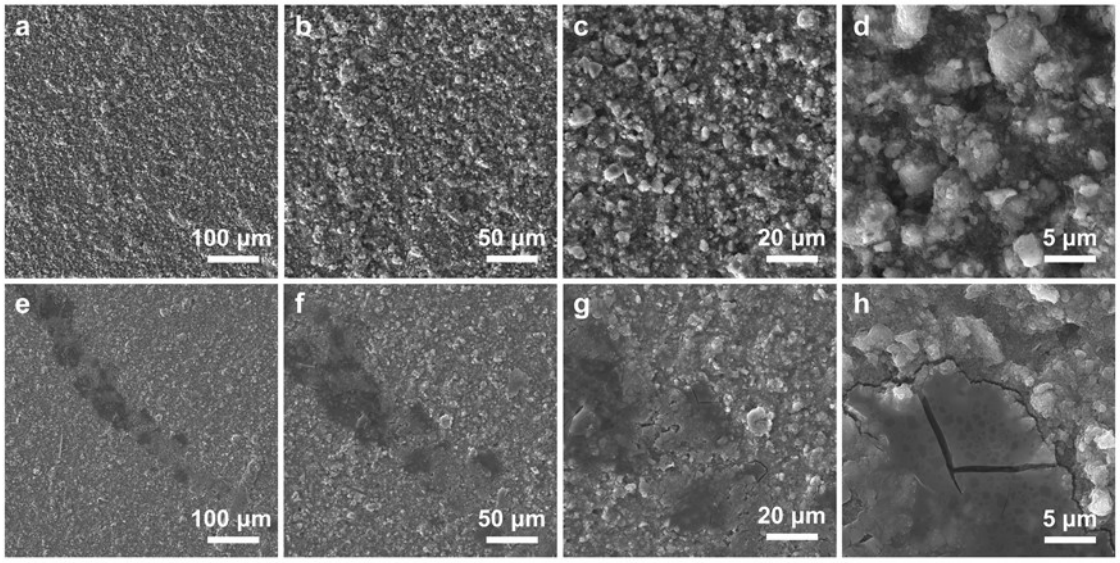

Fig. S8 The SEM images of NFPO-O electrode (a-d) before cycling, and (e-h) after 200 cycles at 5 C.

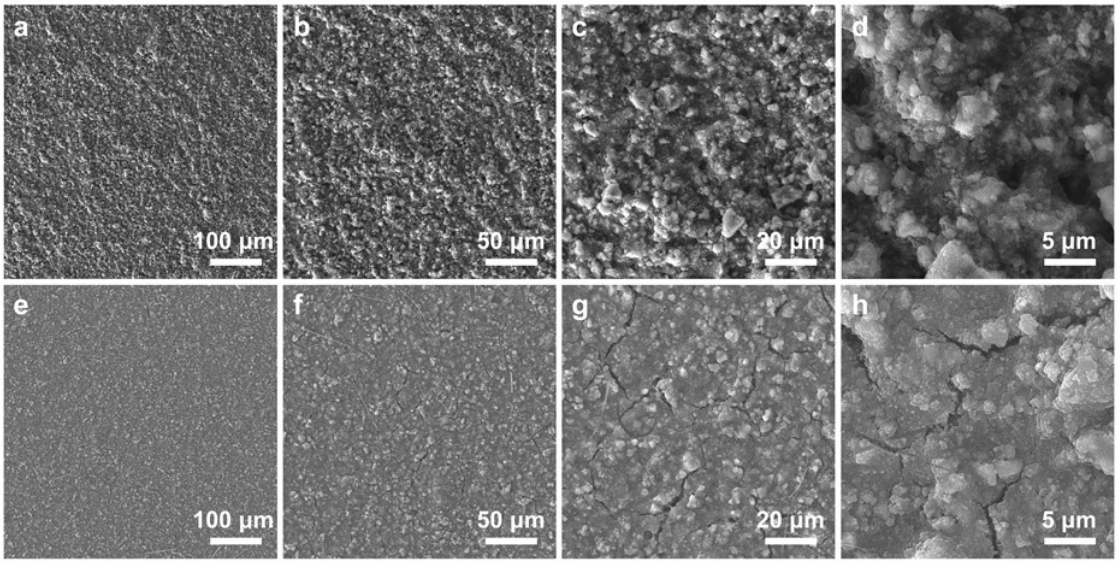

Fig. S9 The SEM images of NFPO-P electrode (a-d) before cycling, and (e-h) after 200 cycles at 5 C.

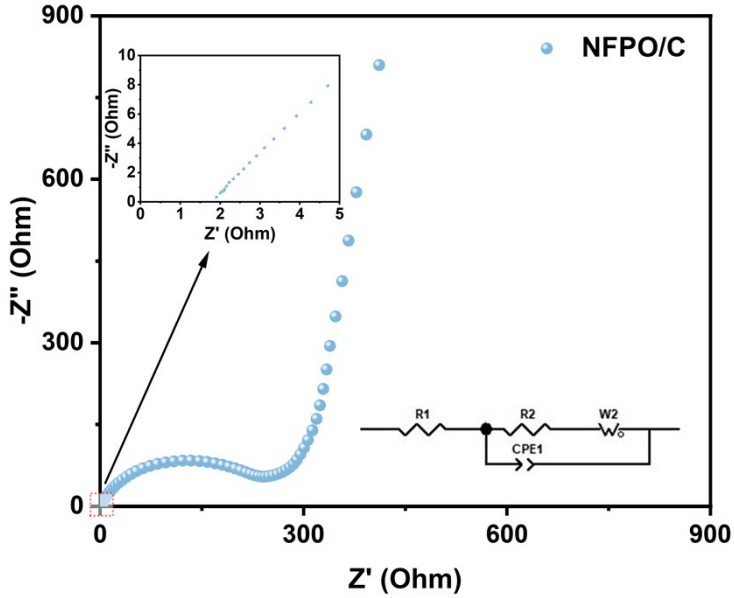

Fig. S10 Nyquist plot of NFPO/C nanoflakes electrode before cycle (three-electrode).

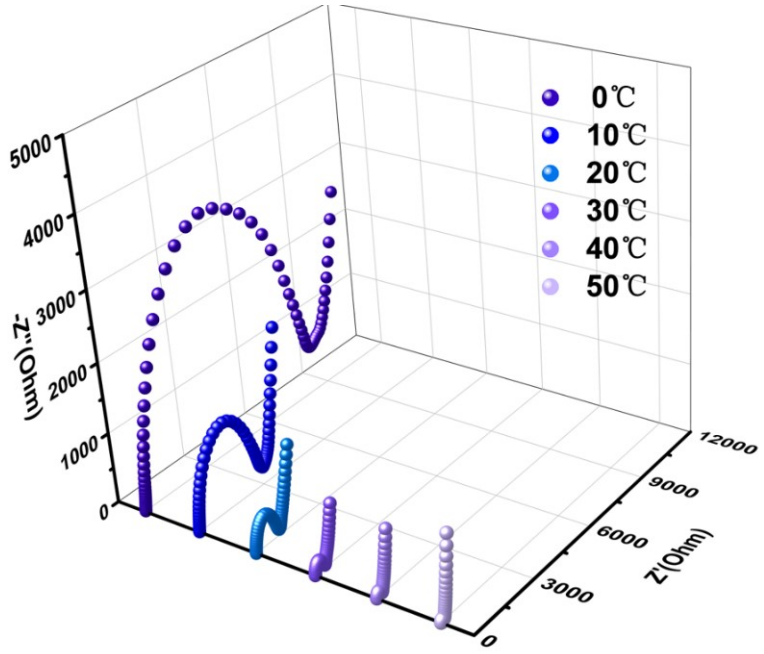

Fig. S11 Nyquist plots of NFPO/C electrodes at different temperatures.

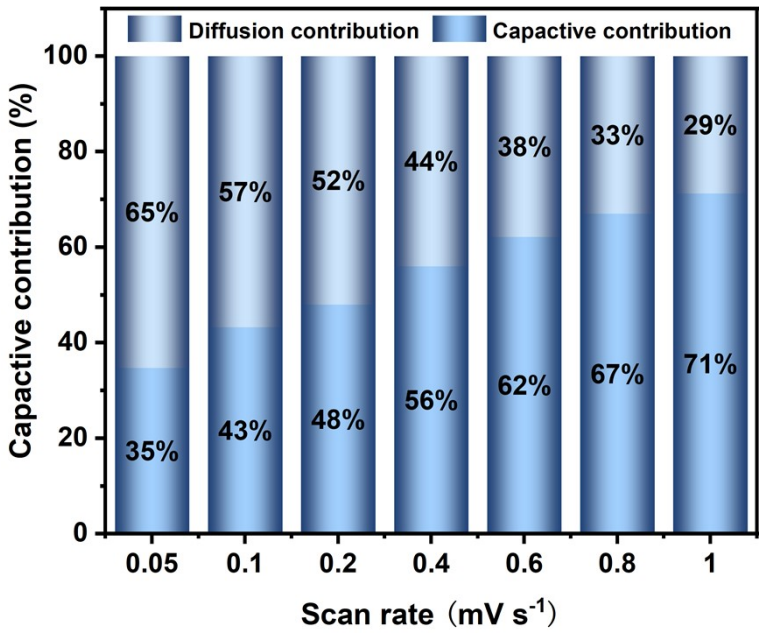

Fig. S12 Normalized contribution ration of capacities at different scan rates for NFPO/C electrodes (two-electrode).

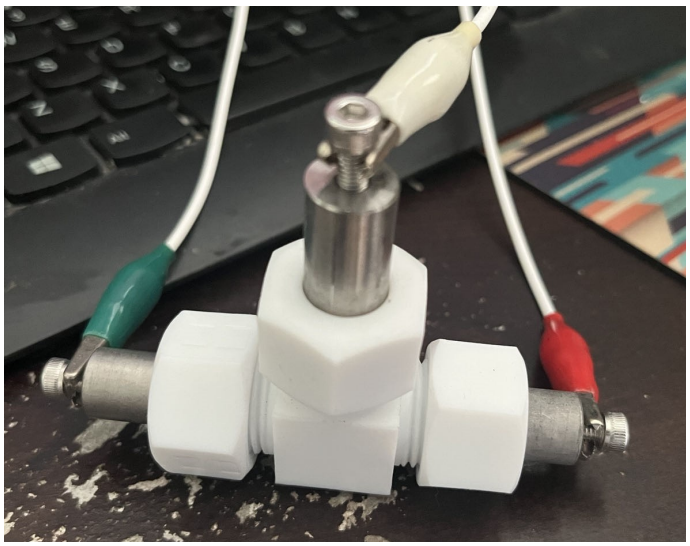

Fig. S13 Swagelok cell system for three-electrode testing.

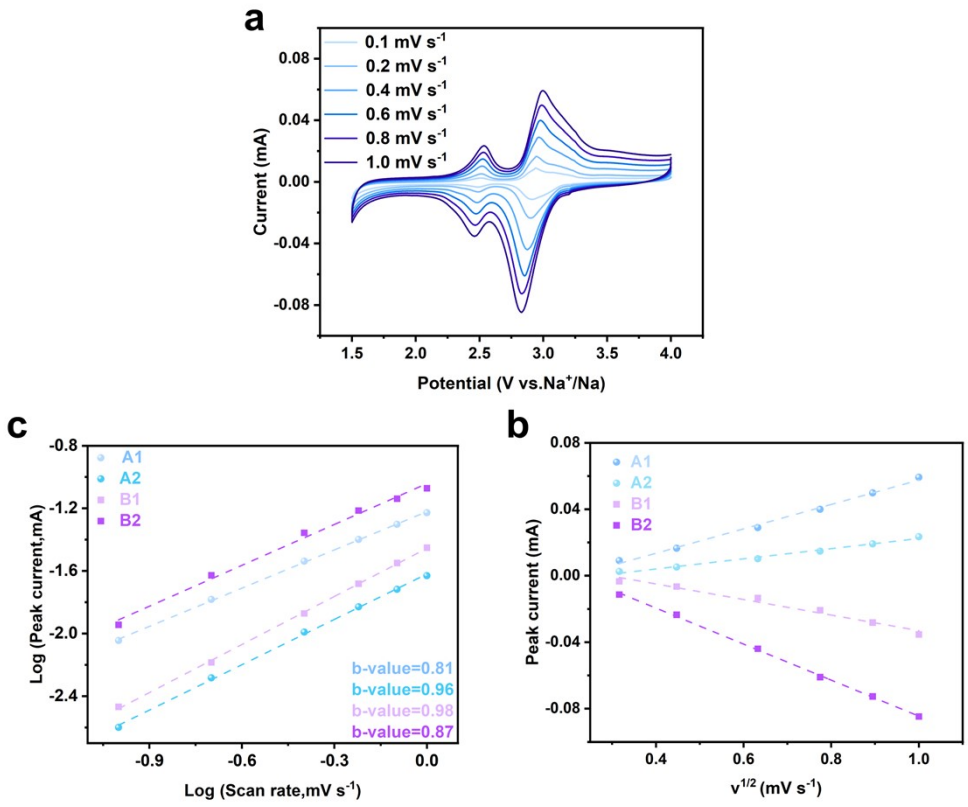

Fig. S14 (a) The CV curves at various scan rates from 0.1 to 1.0 mV s^{-1}(three-electrode). (b) The linear relationship between the peak current and the square root of the scan rate(three-electrode). (c) The Log(v) versus Log (I_p) plots for the different peaks in the CV curves(three-electrode).

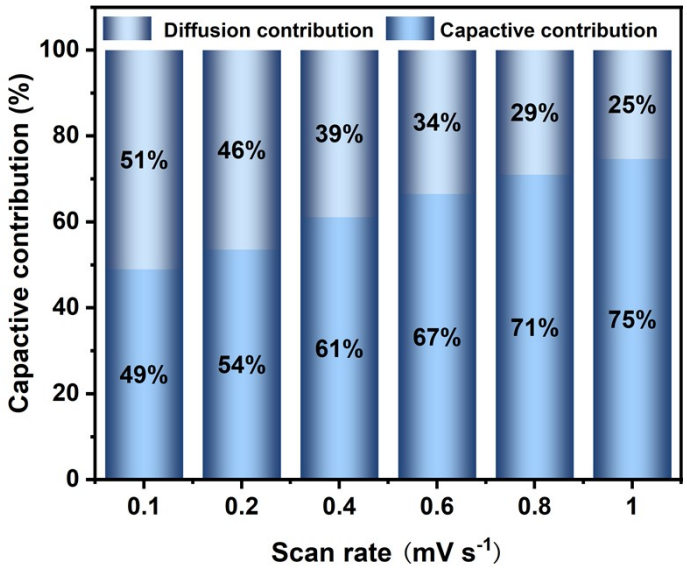

Fig. S15 Normalized contribution ration of capacities at different scan rates for NFPO/C electrodes (three-electrode).

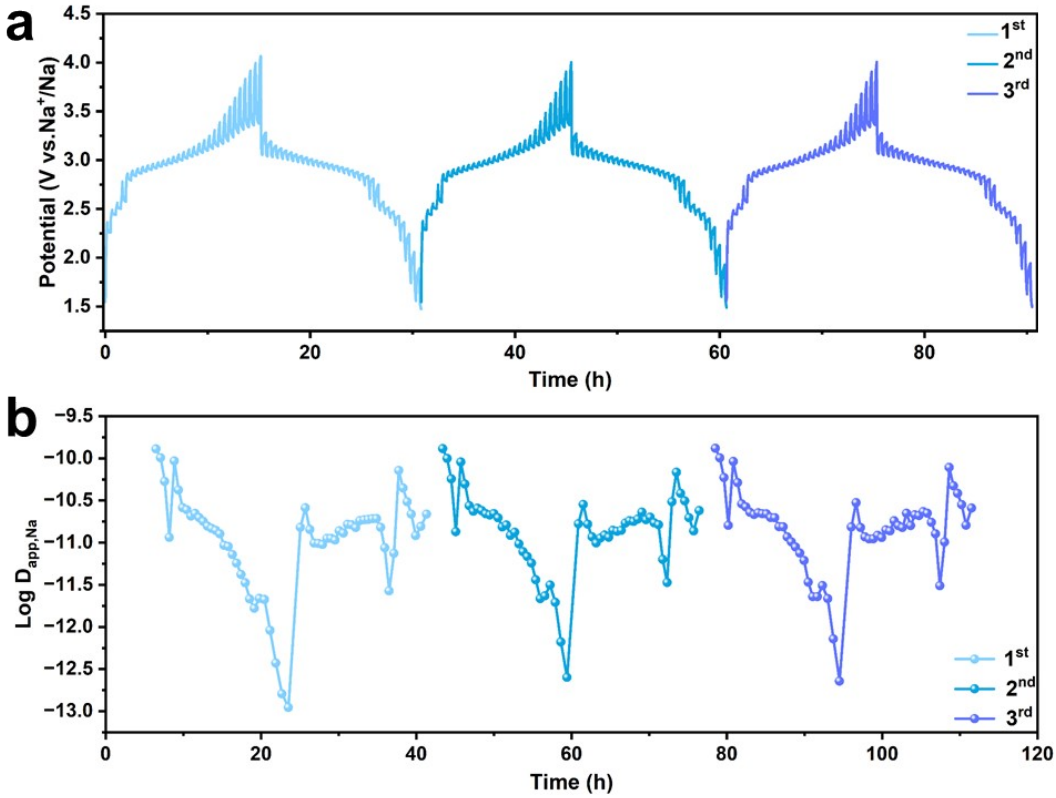

Fig. S16 The GITT curves and corresponding Na^+ diffusion coefficients for the initial three complete charge/discharge processes.

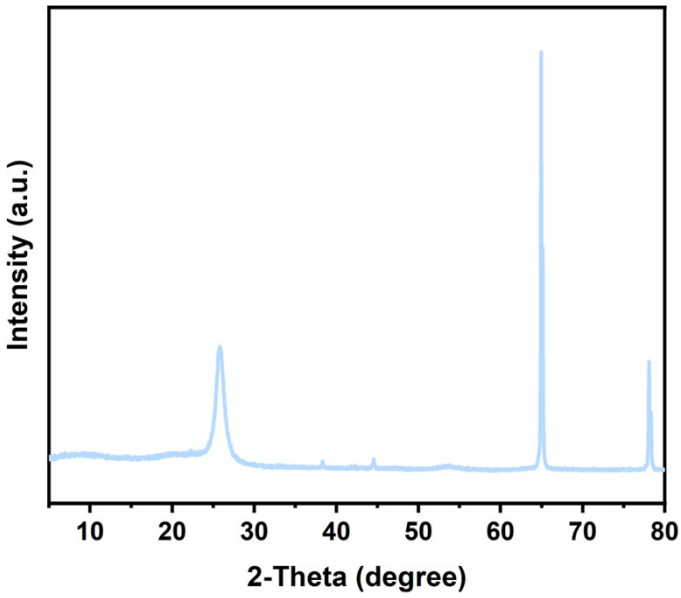

Fig. S17 The XRD pattern of Aluminum foil.

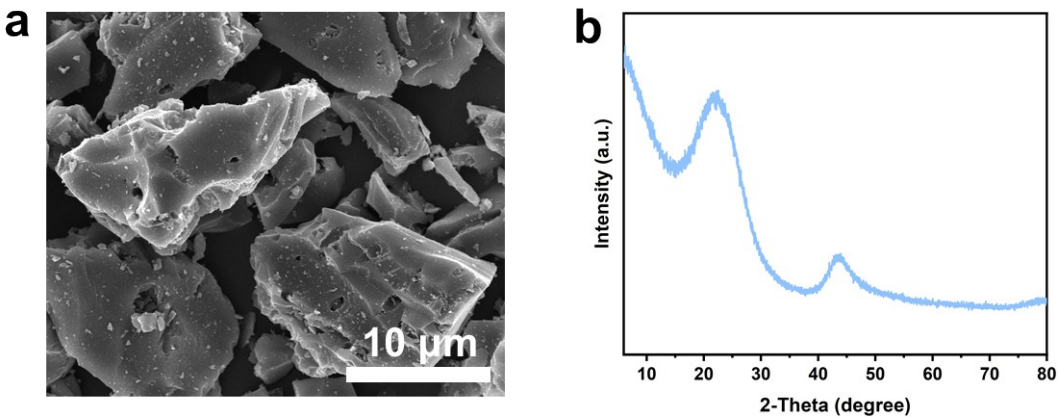

Fig. S18 (a) SEM image, and (b) XRD pattern of hard carbon (HC).

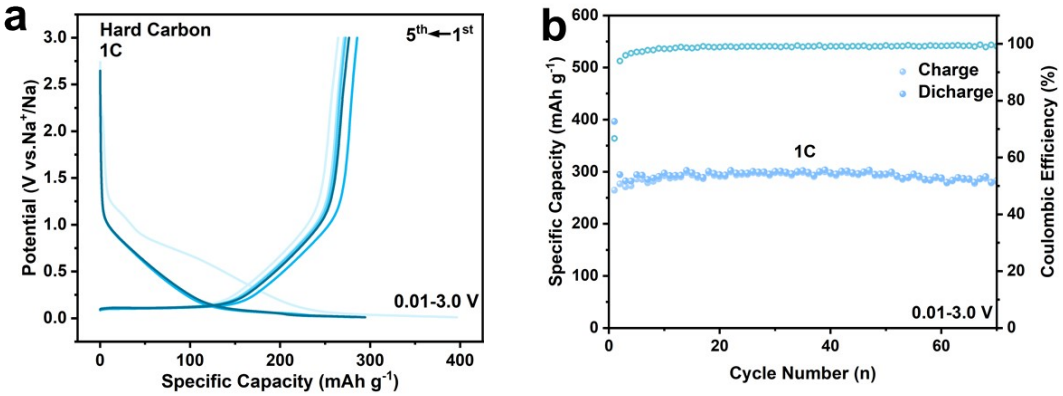

Fig. S19 (a) The initial five charge/discharge profiles, and (b) the cycling performance at 1C for the HC anode.

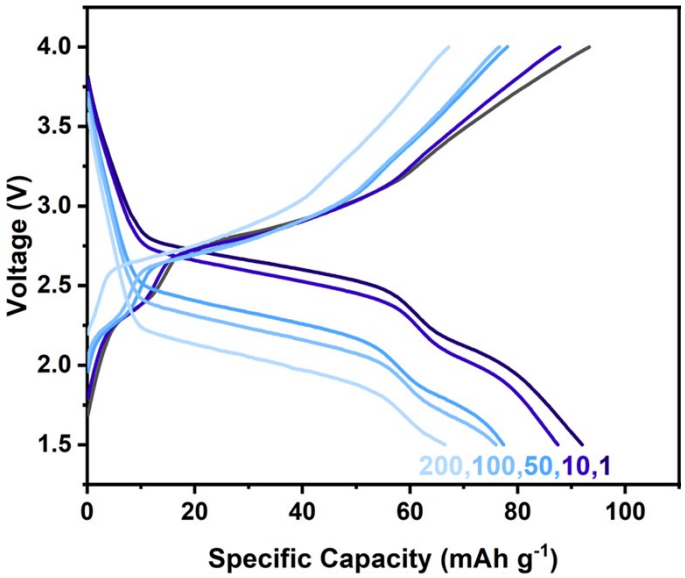

Fig. S20 The charge/discharge profiles of HC//NFPO/C full cell for different number of cycles.

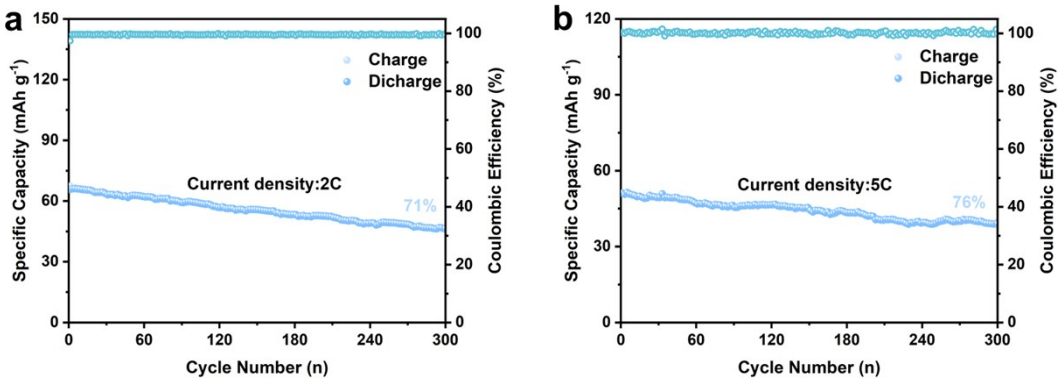

Fig. S21 Cycling performance of HC//NFPO/C full cells at (a) 2C, and (b) 5C.

Table S1. Detailed structural information on $Na_{3.12}Fe_{2.44}(P_2O_7)_2$/C (NFPO/C) after Rietveld refinement.

NFPO/C ($Na_{3.12}Fe_{2.44}(P_2O_7)_2$/C). Space group P-1

a=6.392Å; *b*=9.374Å; *c*=10.955Å

α=64.451°;*β*=85.930°;*γ*=73.088°; *V*=565.440Å

R_{wp}=4.42%; R_p =3.28%; CHI^2=2.322.

Atom	x	y	z	Mult	Occupancy
Fe1	0.355710	0.500344	0.236425	2	1.0000
Fe2	0.277510	0.107744	0.282415	2	1.0000
P1	-0.072690	0.180744	0.710335	2	1.0000
P2	0.289410	0.192344	0.539335	2	1.0000
P3	0.572710	0.704344	-0.043865	2	1.0000
P4	0.876510	0.456144	0.183635	2	1.0000
Fe3	0.795910	0.489644	0 453735	2	0.1180
Fe4	-0.026490	0.185744	0.021335	2	0.3230
O1	0.079810	0.277744	0.599335	2	1.0000
O2	0.769410	0.545144	0 032635	2	1.0000
O11	-0.104490	0.061644	0 659535	2	1.0000
O12	-0.282690	0.313944	0 695735	2	1.0000
O13	0.045910	0.100944	0.846735	2	1.0000
O21	0.438810	0.071444	0 663435	2	1.0000
O22	0 215210	0.109144	0 467435	2	1.0000
O23	0.380410	0.328444	0 446635	2	1.0000
O31	0.647110	0.851544	-0.061565	2	1.0000
O32	0.549610	0.705644	-0.181865	2	1.0000
O33	0380210	0 689644	0.040835	2	1.0000
O41	1.030910	0.546444	0.189535	2	1.0000
O42	0.983110	0.281744	0.202435	2	1.0000
O43	0.691410	0.467444	0 276135	2	1.0000
Na1	0.207810	-0 153156	0 601335	2	1.0000
Na2	0.414710	0.147744	-0.161965	2	1.0000
Na3	0.500000	0.500000	0.500000	1	0.8820
Na4	-0.026490	0.185744	0.021335	2	0.6770

Table S2. ICP test results of NFPO/C sample.

Element	Average concentration (wt%)	Atomic ratio (based on Na)	Sample 1 (wt%)	Sample 2 (wt%)	Sample 3 (wt%)
Fe	27.97	2.677	28.13332	27.92698	27.8366
Na	13.38	3.120	13.43508	13.2686	13.42318
P	22.26	3.853	22.20213	22.38479	22.20268

Table S3. A survey of electrochemical properties of cathodes in this study with previously reported iron-based polyanion compounds.

Cathode	Voltage	Rate Capability	Cycling Ability
Olivine $NaFePO_4$[3]	2.1-3.6V	111 mAh g^{-1} at 0.1C; 46 mAh g^{-1} at 2C	90% after 240 cycles at 0.1C
Olivine $NaFePO_4$[4]	2-4V	142 mAh g^{-1} at 0.1C; 60 mAh g^{-1} at 10C	92% after 200 cycles at 0.1C
Maricite $NaFePO_4$[5]	1.5-4.5V	145 mAh g^{-1} at 0.2C; 61 mAh g^{-1} at 50C	89% after 6300 cycles at 5C
Maricite $NaFePO_4$[6]	1.5-4.5V	149.2 mAh g^{-1} at 0.2C; 75.7 mAh g^{-1} at 50C	95% after 5000 cycles at 10C
Na_2FePO_4F[7]	2-4V	103.2 mAh g^{-1} at 0.1C; 66.8 mAh g^{-1} at 4C	84.7% after 100 cycles at 5C
$Na_{2+2x}Fe_{2-x}(SO_4)_3$/SWNT[8]	2-4.5V	85.3 mAh g^{-1} at 1C; 74.9 mAh g^{-1} at 10C	92% after 1000 cycles at 4C
$Na_2Fe_2(SO_4)_3$/C[9]	1.8-4.2V	107.9 mAh g^{-1} at 0.1C; 75.1 mAh g^{-1} at 10C	90.1% after 300 cycles at 0.2C
$Na_{6-2x}Fe_x(SO_4)_3$[10]	2-4.4V	104.5 mAh g^{-1} at 0.1C; 81.5 mAh g^{-1} at 30C	72.4% after 10000 cycles at 30C
$Na_4Fe_3(PO_4)_2P_2O_7$[11]	1.9-4.1V	113 mAh g^{-1} at 0.05C; 80.3 mAh g^{-1} at 20C	69.1% after 4400 cycles at 20C
$Na_4Fe_{2.95}Mg_{0.05}(PO_4)_2P_2O_7$[12]	1.5-4.2V	104 mAh g^{-1} at 0.05A g^{-1}; 40 mAh g^{-1} at 20A g^{-1}	80.8% after 14000 cycles at 5A g^{-1}
$Na_4Fe_{2.91}(PO_4)_2P_2O_7$[13]	1.7-4.3V	110.9 mAh g^{-1} at 0.2C; 52 mAh g^{-1} at 100C	100% after 10000 cycles at 10C
$Na_4Fe_3(PO_4)_2P_2O_7$[14]	1.7-4.3V	118 mAh g^{-1} at 0.2C; 64 mAh g^{-1} at 20C	79.6% after 10000 cycles at 10C
$Na_{3.9}Fe_{2.9}Al_{0.1}(PO_4)_2(P_2O_7)$[15]	1.7-4.3V	114.5 mAh g^{-1} at 0.1C; 41.7 mAh g^{-1} at 200C	85.1% after 10000 cycles at 50C

Table S4. Impedance parameters from the fitting equivalent circuit.

Samples	R1	R2	W2-R	W2-T	W2-P	CPE1-T	CPE1-P
NFPO/C	1.907	207.1	262.5	1.166	0.4492	3.5682×10^{-5}	0.82099
Error (%)	1.9168	1.8873	8.8891	11.262	1.0935	4.4616	0.5964

Note S1

In this work, the carbon content of the prepared cathode materials can be calculated based on the following two equations:

$$\mathbf{C+O_2=CO_2}$$

$$\mathbf{Na_{3.12}Fe_{2.44}(P_2O_7)_2+ nO_2\rightarrow Na_3Fe_2(PO_4)_3+NaFeP_2O_7}$$

All calculations of carbon content were based on the law of conservation of mass as well as the law of conservation of charge. The formula is: carbon content (%) = 8.5% + (1 - 8.5%) × [(2.44/4 × M_{O2}) ÷ M_{NFPO}], where M_{O2} and M_{NFPO} are the relative molecular mass of O_2 and NFPO, respectively.

Note S2

In this work, the following two equations are used to fit the activation energy:

$i_0 = RT/nFR_{ct}$

$i_0 = Aexp(-Ea/RT)$

where *A* is a temperature independent coefficient, *R* is the gas constant, *T* (K) is the absolute temperature, *n* is the number of transferred electrons, and *F* is the Faraday constant.

Note S3

In this work, the diffusion coefficient of sodium ions for the NFPO/C cathode is calculated by the following typical Randles-Sevcik equation:

$$I_P = 2.69 \times 10^5 n^{3/2} A D^{1/2} v^{1/2} C_0^*$$

where I_p is the peak current (A), n is the number of electron transfers, A is the contact area of the electrode with the electrolyte, D is the diffusion coefficient of the sodium ion ($cm^2\ s^{-1}$), v is the scanning rate ($V\ s^{-1}$), and C_0^* is the bulk concentration of sodium ion in electrode ($mol\ cm^{-3}$).

Note S4

In this work, the charge storage mechanism of the NFPO/C cathode is discussed according to the following equation:

$$i = av^b$$

$$logi = b \times logv + loga$$

where i is the current density, v is the scan rate, and a and b are adjustable parameters. When the value of b is 1, it represents the capacitive response, and when the value of b is around 0.5, it represents the diffusion-limited response.

Reference

1. X. Cao, A. Pan, S. Liu, J. Zhou, S. Li, G. Cao, J. Liu and S. Liang, *Adv. Energy Mater.*, 2017, **7**.

2. S. Liang, X. Cao, Y. Wang, Y. Hu, A. Pan and G. Cao, *Nano Energy*, 2016, **22**, 48-58.

3. Y. Fang, Q. Liu, L. Xiao, X. Ai, H. Yang and Y. Cao, *ACS Appl. Mater. Interfaces*, 2015, **7**, 17977-17984.

4. W. Tang, X. Song, Y. Du, C. Peng, M. Lin, S. Xi, B. Tian, J. Zheng, Y. Wu, F. Pan and K.

P. Loh, *J. Mater. Chem. A*, 2016, **4**, 4882-4892.

5. Y. Liu, N. Zhang, F. Wang, X. Liu, L. Jiao and L.-Z. Fan, *Adv. Funct. Mater.*, 2018, **28**, 1801917.

6. B. Liu, Q. Zhang, L. Li, L. Zhang, Z. Jin, C. Wang and Z. Su, *Chem. Eng. J.*, 2021, **405**, 126689.

7. X. Deng, W. Shi, J. Sunarso, M. Liu and Z. Shao, *ACS Appl. Mater. Interfaces*, 2017, **9**, 16280-16287.

8. Y. Meng, T. Yu, S. Zhang and C. Deng, *J. Mater. Chem. A*, 2016, **4**, 1624-1631.

9. M. Chen, D. Cortie, Z. Hu, H. Jin, S. Wang, Q. Gu, W. Hua, E. Wang, W. Lai, L. Chen, S.-L. Chou, X.-L. Wang and S.-X. Dou, *Adv. Energy Mater.*, 2018, **8**, 1800944.

10. A. Zhao, F. Ji, C. Liu, S. Zhang, K. Chen, W. Chen, X. Feng, F. Zhong, X. Ai, H. Yang, Y. Fang and Y. Cao, *Sci. Bull.*, 2023, **68**, 1894-1903.

11. M. Chen, W. Hua, J. Xiao, D. Cortie, W. Chen, E. Wang, Z. Hu, Q. Gu, X. Wang, S. Indris, S.-L. Chou and S.-X. Dou, *Nat. Commun.*, 2019, **10**, 1480.

12. F. Xiong, J. Li, C. Zuo, X. Zhang, S. Tan, Y. Jiang, Q. An, P. K. Chu and L. Mai, *Adv. Funct. Mater.*, 2023, **33**, 2211257.

13. A. Zhao, T. Yuan, P. Li, C. Liu, H. Cong, X. Pu, Z. Chen, X. Ai, H. Yang and Y. Cao, *Nano Energy*, 2022, **91**, 106680.

14. W. Ren, M. Qin, Y. Zhou, H. Zhou, J. Zhu, J. Pan, J. Zhou, X. Cao and S. Liang, *Energy Storage Mater.*, 2023, **54**, 776-783.

15. J. Gao, J. Zeng, W. Jian, Y. Mei, L. Ni, H. Wang, K. Wang, X. Hu, W. Deng, G. Zou, H. Hou and X. Ji, *Sci. Bull.*, 2024, **69**, 772-783.